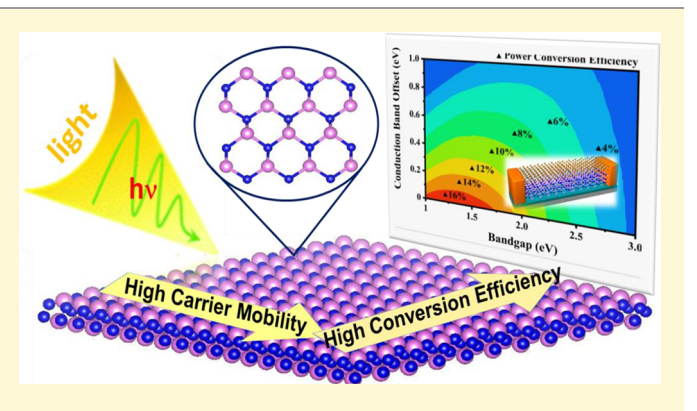


# Identifying the Ground-State NP Sheet through a Global Structure Search in Two-**Dimensional Space and Its Promising High-Efficiency Photovoltaic Properties**

Yuanzheng Chen,\*,<sup>†,‡,</sup>√<sup>⑤</sup> Zebin Lao,<sup>†,</sup>√ Bai Sun,<sup>†,¶,</sup>√<sup>⑥</sup> Xiaolei Feng,\*,<sup>§,∥,</sup> Simon A. T. Redfern,<sup>§,∥,</sup> Hanyu Liu,<sup>⊥</sup> Jian Lv,<sup>#</sup> Hongyan Wang,<sup>†</sup> and Zhongfang Chen\*,<sup>□,</sup>

Supporting Information

ABSTRACT: Recently fabricated two-dimensional (2D) black phosphorene (BP) is considered to be a promising optoelectronic sheet, but its applications are hindered by the poor stability in air. Thus, it is desirable to investigate other BP-like 2D materials, which may have improved stability, while preserving the exceptional electronic properties of BP. Herein, using an efficient structure search method, we predicted a novel 2D BP-like material, namely, a honeycomb NP sheet ( $\alpha$ -NP). Remarkably, its few-layer  $\alpha$ -NP sheets possess not only a tunable direct bandgap under in-plane strain but also high mobility (×10<sup>4</sup> cm<sup>2</sup> V<sup>-1</sup> s<sup>-1</sup>) and absorption coefficients ( $\times 10^5$  cm<sup>-1</sup>). These advantageous characteristics endow the  $\alpha$ -NP sheets



as a very potential 2D material for efficient photovoltaic cell applications, as demonstrate by an estimated photovoltaic efficiency of  $\sim$ 14%, when its thickness is at  $\sim$ 1  $\mu$ m. When combined with 2D MoTe<sub>2</sub>, it can provide a type-II heterojunction solar cell with a conversion efficiency up to ~16%. We also proposed a feasible strategy for mechanical cleavage to prepare the  $\alpha$ -NP sheets from its bulk NP compound. Once prepared, the  $\alpha$ -NP sheets may offer superior photovoltaic properties and facilitate the development of solar cells and optoelectronic devices.

onverting solar energy into electrical power using semiconductor materials is very promising to satisfy the ever-increasing demand for renewable energy. 1,2 Many bulk inorganic semiconductor materials, such as Si, GaAs, CdTe,<sup>3-6</sup> and conjugated polymers,<sup>7-9</sup> have been utilized, with varying degrees, as solar energy convertors. Compared with these traditional bulk semiconductor materials, two-dimensional (2D) semiconductors offer a promising

alternative for the feasible construction of ultrathin solar cells with high conversion efficiency and flexibility. 10 Such 2D semiconductor materials typically have large contact areas for optical absorption, which could be straightforwardly engi-

Received: June 14, 2019 Accepted: August 20, 2019 Published: August 20, 2019



<sup>&</sup>lt;sup>†</sup>School of Physical Science and Technology, Key Laboratory of Advanced Technologies of Materials, Southwest Jiaotong University, Chengdu 610031, China

<sup>&</sup>lt;sup>‡</sup>Beijing Computational Science Research Center, Haidian District, Beijing 100193, China

<sup>§</sup>Department of Earth Sciences, University of Cambridge, Downing Street, Cambridge, CB2 3EQ, UK

Center for High Pressure Science and Technology Advanced Research (HPSTAR), Shanghai 201203, P. R. China

<sup>&</sup>lt;sup>1</sup>Innovation Center for Computational Physics Methods and Software, College of Physics, Jilin University, Changchun 130012,

<sup>\*</sup>College of Materials Science and Engineering, Jilin University, Changchun 130012, China

<sup>&</sup>lt;sup>¶</sup>Department of Mechanics and Mechatronics Engineering, Centre for Advanced Materials Joining, Waterloo Institute for Nanotechnology, University of Waterloo, Waterloo, Ontario N2L 3G1, Canada

Department of Chemistry, University of Puerto Rico, Rio Piedras Campus, San Juan, Puerto Rico 00931, United States

neered with tunable optoelectronic properties such as high carrier mobility. For example, the 2D sp<sup>2</sup>-hybridized carbon monolayer, namely, graphene, <sup>11</sup> possesses a very high carrier mobility up to  $\sim \! 10^5$  cm<sup>2</sup>/V/s. Various heterojunction solar cells made from graphene have been proposed, including graphene/BN<sup>12</sup> and graphene/MoS<sub>2</sub>. <sup>12</sup> Solar cells based on 2D semiconductor materials are currently of significant interest owing to their apparent high performance and suitability in a wider variety of applications compared to traditional Si solar cells.

In 2014, a novel 2D semiconductor material, namely, black phosphorene (BP), <sup>13</sup> was successfully fabricated. It has a comparatively high carrier mobility of 10<sup>4</sup> cm<sup>-2</sup>/V/s and a broad direct bandgap (1.1–2 eV), depending on the number of its layers. <sup>14</sup> Because of its bandgap tunability and its puckered geometric structure, certain properties of BP, such as its layer-dependent bandgap and ambipolar conduction characteristics, are even superior to graphene. For example, BP as a promising material has a drain current modulation of up to 10<sup>5</sup> in optoelectronics device applications; <sup>13,15</sup> BP is also an ideal 2D material for photovoltaic applications. Despite these advantages, the practical applications of BP are seriously restricted by its poor stability in air, since the oxidation by oxygen O<sub>2</sub> atmosphere <sup>16</sup> leads to rapid degradation of the performance.

Recently, some theoretical and experimental researches about 2D P-based materials suggested that the BP analogues are useful alternatives with good stability in air and have an application prospect in photovoltaics. 17-25 For example, Zeng and coworkers indicate the  $\alpha$ -AsP has a good stability and can be used to construct solar cells ( $\alpha$ -AsP/GaN) with power conversion efficiency (PCE) approaching to 22%. <sup>17</sup> In addition, recent first-principles studies suggest that the atomic and electronic structure of BP can be modulated by N and B doping, especially N doping can decrease the chemical activity of BP.<sup>26</sup> Using first-principles methods (e.g., structure searching and high-throughput screening), various 2D materials<sup>27-29</sup> and several 2D monolayer phases of nitridephosphorus (N–P) system<sup>30–32</sup> with fantastic structures and properties have been proposed and investigated. These exciting theoretical findings and the substantial promise of the new 2D P-based materials for solar cells inspired us to investigate the stability, electronic and optical properties, and photovoltaics applications of N-P sheets.

Here, we performed a systematic exploration of the low-lying structures of monolayer N-P polymorphs with various stoichiometries by adopting an intelligence structure-searching method of particle-swarm optimization.<sup>33</sup> Our exhaustive search revealed a low-lying BP-like monolayer (denoted  $\alpha$ -NP) with N: P = 1:1 composition. This  $\alpha$ -NP monolayer is predicted to have remarkable thermal stability and good dynamical structural stability. Notably, the  $\alpha$ -NP sheets are rather promising for photovoltaic applications, as indicated by the modulated direct bandgap upon compression, high carrier mobility, and high absorption coefficients. The estimated photovoltaic efficiency of  $\alpha$ -NP sheet material as a function of the thickness and the conversion efficiency of  $\alpha$ -NP sheetbased heterojunction solar cell confirmed its high-efficiency photovoltaic applications. Our results also revealed that the  $\alpha$ -NP sheet could be prepared by mechanical cleavage from our predicted bulk NP structure.

We performed searches for stable structures of 2D N-P sheets  $N_x P_{1-x}$  (x = 3/4, 2/3, 3/5, 1/2, 2/5, 1/3, and 1/4) and

the bulk structure of the NP compound at 0-10 GPa using the PSO structure-searching method implemented in the CALYP-SO code,<sup>33</sup> which had been benchmarked on various systems and compounds.34-41 The geometric optimizations and electronic structure calculations were performed within the generalized gradient approximation (GGA) using VASP code. 42 The van der Waals density functional 43 was adopted to treat interaction between adjacent layers in multilayer structure. A vacuum space of 20 Å along the z direction was set to avoid the interaction between repeat images of the neighboring N-P monolayer. In first-principles calculation, the cut-off energy is set to 800 eV, the reciprocal space grid of  $0.025 \times 2\pi \text{ Å}^{-1}$  is chosen for the Brillouin-zone sampling, and the convergence threshold for the total energy and the force are set as  $1 \times 10^{-5}$  eV and 0.01 eV/Å, respectively. The Heyd-Scuseria-Ernzerhof (HSE) hybrid functional<sup>44</sup> was adopted to accurately describe the bandgap. The phonon dispersion calculation was performed by adopting the supercell method using the PHONOPY code. 45 Ab initio molecular dynamics (AIMD) simulations were carried out at 300, 1000, and 1500 K in the canonical ensemble. The details for the computational methods of carrier mobility, absorption coefficients, and power conversion efficient are given in the Supporting Information.

Combining the first-principles calculations with PSO approach, we performed a comprehensive study to explore the monolayer  $N_x P_{1-x}$  materials with typical compositions. The thermodynamic stability of monolayer  $N_x P_{1-x}$  was evaluated by computing their formation energies, defined as  $\Delta E(N_x P_{1-x}) = E(N_x P_{1-x}) - xE(N) - (1-x)E(P)$ . Here, the experimentally synthesized phosphorene 13 and theoretically predicted nitrogene 46 were used to calculate the elemental energy of E(P) and E(N). When any structure with its formation energy is on the convex hull, it is deemed to be thermodynamically stable and experimentally feasible. Checking plot of the formation energies versus N concentrations (Figure 1a), we found a global minimum structure in this 2D space at the mid-point with N: P = 1:1, which comprises a corrugated honeycomb

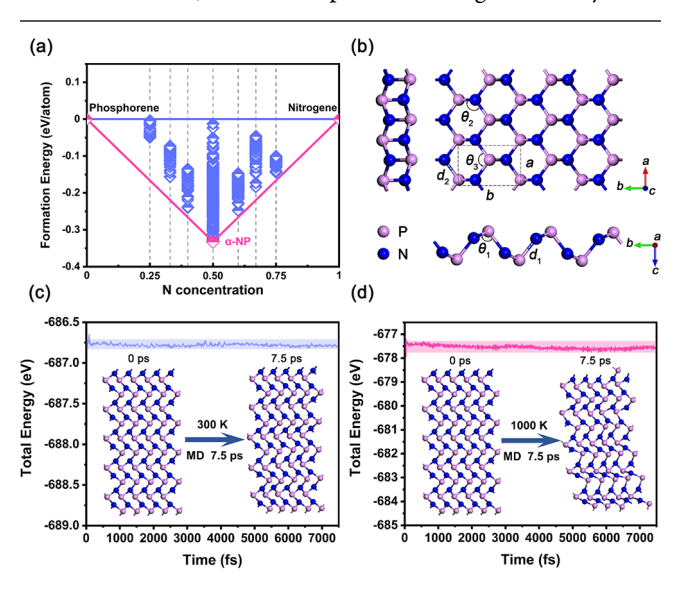


Figure 1. (a) Computed formation energy vs the nitrogen concentration for the N–P monolayers. The convex hull is labeled by the red solid line. (b) The structure symmetry of  $\alpha$ -NP monolayer from the side, top, and front views. (c and d) The structure and total-energy evolution for  $\alpha$ -NP monolayer in AIMD simulations at  $T=300~{\rm K}$  (c) and  $1000~{\rm K}$  (d), respectively.

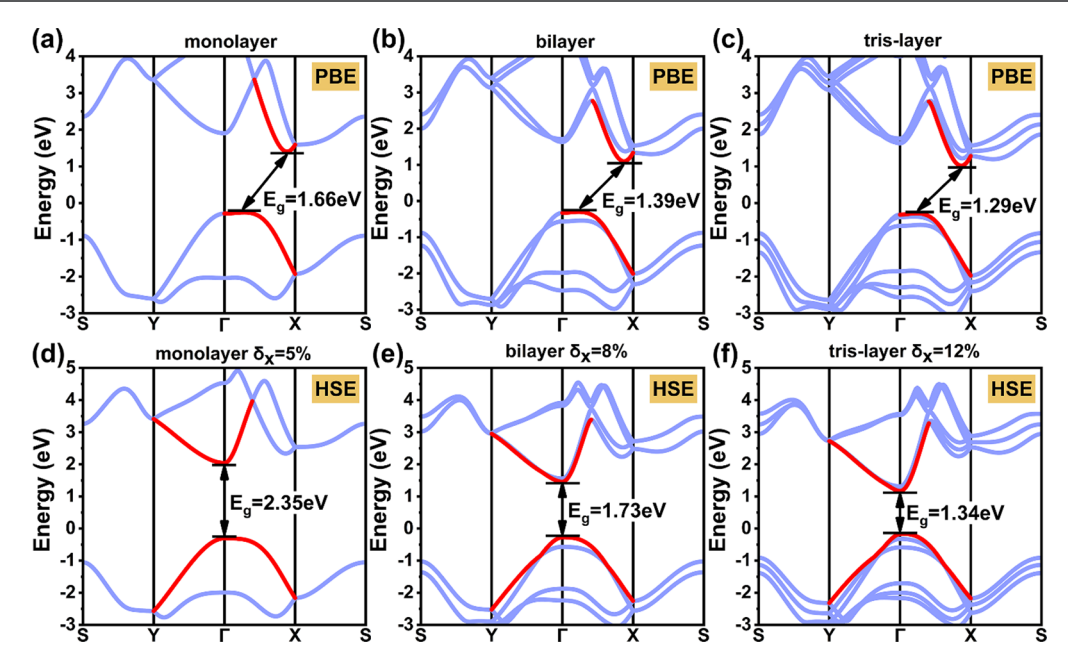


Figure 2. Calculated band structures of the 1L  $\alpha$ -NP (a), 2L  $\alpha$ -NP (b), and 3L  $\alpha$ -NP (c) using the PBE functional level. The computed band structures at a strain value of  $\delta_x$  = 5% for the 1L  $\alpha$ -NP (d),  $\delta_x$  = 8% for the 2L  $\alpha$ -NP (e), and  $\delta_x$  = 12% for the 3L  $\alpha$ -NP (f) by HSE functional level.

structure very similar to that of BP. Note that structurally this configuration is consistent with the  $\alpha$ -configuration computationally designed by Zhang and coworkers;<sup>30</sup> thus, we denoted it as  $\alpha$ -NP (Figure 1b). To further check the structural stability of the  $\alpha$ -NP sheet, we calculated its cohesive energy  $(E_c)$ defined as  $E_c = [E(N) + E(P) - E(\alpha - NP)]/2$ , where E(N), E(P), and  $E(\alpha-NP)$  are the total energies of a single N atom, a single P atom, and one unit cell of the  $\alpha$ -NP monolayer, respectively. The calculated  $E_c$  value of  $\alpha$ -NP (~4.69 eV/ atom) is larger than that of BP (3.48 eV/atom), indicating that the bonding in  $\alpha$ -NP sheet is more robust than that in BP. Compared with several known monolayer PN structures, this  $\alpha$ -NP sheet is much lower in energy than the  $\beta$  and  $\gamma$ configurations and is energetically very close to  $P2_1/c$ -NP with a difference of  $\sim$ 0.02 eV/atom. <sup>30-32</sup> In these PN monolayer allotropes, the low-energy  $\alpha$ -NP and  $P2_1/c$ -PN structures seem to the highly feasible for experimental realization. Especially, here, the  $\alpha$ -NP is revealed to can be exfoliated from its bulk NP compound as discussed later, thus the  $\alpha$ -NP structure is the focus of our exploration from its properties to applications by dependence on few-layers in the following sections.

Structurally, the  $\alpha$ -NP sheet well resembles the corrugated structure of BP, which can be constructed by simply replacing alternative P atoms in the hexagonal unit of BP by N atoms (Figure 1b). In each unit cell, the  $\alpha$ -NP sheet consists of four atoms, and its optimized lattice parameters are a = 2.700 Å, b = 2.700 Å=4.164 Å,  $d_1$ = 1.820 Å,  $d_2$  = 1.723 Å, 9b07514 = 97.64°,  $\theta_2$  = 123.69°, and  $\theta_3 = 103.14^\circ$ . Both P and N atoms prefer the sp<sup>3</sup> hybridization and form 3-fold coordinated configurations. Its electron localization functions (ELF) and density of states (DOS) (Figure S1) confirm this configuration with a honeycomb covalent bonding characteristics. From the side view as shown in Figure 1b, the cross-section of the  $\alpha$ -NP monolayer also closely resembles the special armchair ridges of BP, the origin of anisotropy in BP. In comparison with BP, the N atoms of  $\alpha$ -NP sheet at three alternating corners of a hexagon are slightly displaced towards its center, while the P

atoms lie above or below its plane with a much smaller buckling distance of  $\sim 0.6$  Å ( $\sim 2.0$  Å in BP).

To assess the dynamic stability of our predicted  $\alpha$ -NP structure, using the finite-displacement method, we calculated its phonon dispersion curves (Figure S2). We found that there are no phonons with imaginary frequencies in the first Brillouin zone of this structure, revealing its dynamical stability. We also examined the mechanic stability of  $\alpha$ -NP sheet by calculating its elastic constants. The elastic constants obtained by the strain-energy method are  $C_{11} = 208.33$ ,  $C_{22} = 39.74$ ,  $C_{12} =$ 23.23, and  $C_{66}$  = 48.77 N/m, respectively. Clearly, the Born–Huang criteria<sup>47</sup> for a mechanically stable 2D material (e.g.,  $C_{11} > C_{12}$ ,  $C_{11}C_{22} - C_{12}^2 > 0$ ,  $C_{66} > 0$ ) can be satisfied in the case of the  $\alpha$ -NP sheet, indicating its mechanical stability. Meanwhile, we evaluated its thermal stability by performing AIMD simulations in the canonical ensemble at 300, 1000, and 1500 K, respectively. At each chosen temperature, the AIMD simulation ran for up to 7.5 ps with a  $4 \times 4 \times 1$  supercell. The total energy with simulation step and the final equilibrium  $\alpha$ -NP structure at each temperature are depicted in Figure 1c and 1d. At 300 and 1000 K, the  $\alpha$ -NP monolayer well maintains its structural integrity, with only slight deformation at 1000 K. However, when T increases to 1500 K, the framework eventually collapses (Figure S3), suggesting that the melting point of  $\alpha$ -NP sheet is at between 1000 and 1500 K. In addition, we performed AIMD simulations at 300 K in an O2 atmosphere (Figure S4). After structural relaxation of 7.5 ps, the  $\alpha$ -NP sheet retains its initial configuration, indicating its remarkable chemical stability. The good chemical stability of the  $\alpha$ -NP sheet may be ascribed to its special buckled P-N hexagon structure, which is not favorable to the formation of bridge P-O-P bonds as seen in BP<sup>16</sup> (Figure S5) during the oxidation process.

Because of the interlayer vdW interactions, the 2D materials usually possess layer-number-dependent electronic properties as exemplified by graphene, <sup>48</sup> BP, <sup>49</sup> and antimonene. <sup>50</sup> To research the electronic properties of the  $\alpha$ -NP sheets, we

ACS Materials Letters

Table 1. Computed Deformation Potential Constant  $(E_d^{\alpha})$ , 2D Elastic Modulus  $(C^{2D})$ , Effective Mass  $(m^*)$ , and Mobility  $(\mu)$  of Electrons and Holes along x (Zigzag) and y (Armchair) Directions for the  $\alpha$ -NP Sheets

$\alpha$ -NP sheets		$m_x^*/m_0$	$m_y^*/m_0$	$C_x^{\mathrm{2D}} \left( \mathrm{N} \ \mathrm{m}^{-1} \right)$	$C_y^{\rm 2D} \ ({\rm N} \ {\rm m}^{-1})$	$E_{\rm d}^x$ (eV)	$E_{\rm d}^y~({ m eV})$	$\mu_x \text{ (cm}^2 \text{ V}^{-1} \text{ s}^{-1}\text{)}$	$\mu_y \text{ (cm}^2 \text{ V}^{-1} \text{ s}^{-1})$
1L	e	0.18	4.47	205.12	40.41	4.29	0.46	$4.9 \times 10^{3}$	135.98
	h	1.88	0.47	205.12	40.41	1.88	2.44	233.06	435.20
2L	e	0.35	1.47	208.42	38.68	3.86	1.79	$1.6 \times 10^{3}$	79.35
	h	3.41	0.55	208.42	38.68	2.04	0.32	61.37	$1.7 \times 10^4$
3L	e	0.17	0.54	312.22	56.86	3.68	1.66	$1.1 \times 10^{4}$	135.98
	h	1.29	0.24	312.22	56.86	2.19	0.57	546.55	$4.2 \times 10^4$

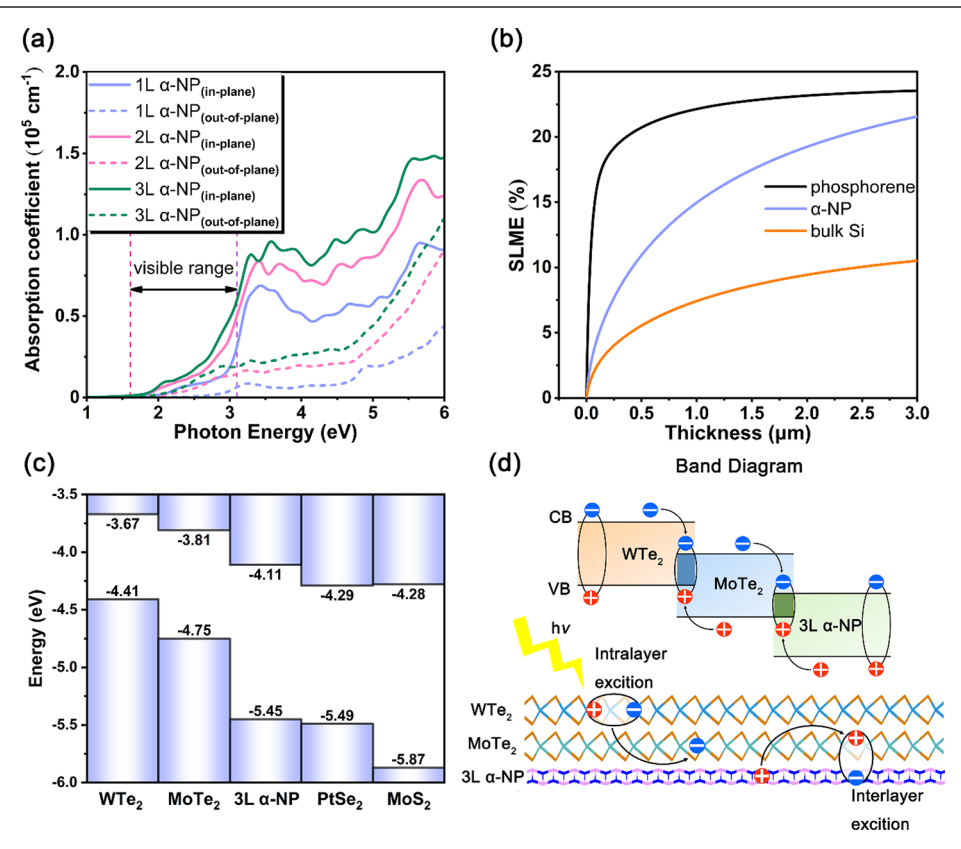


Figure 3. (a) In- and out-of-plane absorption spectra for the 1L, 2L, and 3L  $\alpha$ -NP sheets at the PBE functional level. (b) The calculated SLME as a function of slab thickness for the  $\alpha$ -NP sheet, BP, and bulk silicon. (c) The band alignment of 3L  $\alpha$ -NP and TMDS monolayers. (d) Schematic of electron-hole separation for the WTe<sub>2</sub>-MoTe<sub>2</sub>-3L  $\alpha$ -NP heterostructures.

adopted few layers, such as monolayer (1L), bilayer (2L), and trilayer (3L) and examined their the most important electronic parameter: the band gap. As shown in Figure 2a–2c, the 1L  $\alpha$ -NP is semiconducting with an indirect band gap, the calculated band gap value is 1.66 eV by PBE functional and 2.71 eV by the more accurate HSE functional (Figure S6). When the layers increase to 3L, the band gap decreases almost linearly to 1.29 eV by PBE functional (1.31 eV by HSE functional, Figure S7). These results indicate that the band gap of  $\alpha$ -NP sheets is also dependent on its number of layers.

The electronic band structure was experimentally verified to can be effective modulated by adopting a method of compressive or tensile strains. This is especially pertinent to 2D materials since they can rather easily accommodate significant strain effects, which may be operated by a lattice mismatch with the substrate or slight mechanical loading. To explore this issue, we performed band gap calculations for 1L  $\alpha$ -NP using imposed uniaxial compressive and tensile strain. As seen in Figure S8, the bandgap of 1L  $\alpha$ -NP can be flexibly tuned via strain engineering and correlates nearly linear with

the isotropic strain  $\delta$  in either the x or y direction. Through inspection of its band structure, we speculate that the conduction band minimum (CBM) and the valence band maximum (VBM) can be moved slightly along  $\Gamma \to X$  or  $\Gamma \to X$ Y by giving a uniaxial strain along the x or y direction. Through our calculations with increasing the compressive strain along the x direction, the flat band of VBM along  $\Gamma \to X$  scarcely moved while the conduction band at the  $\Gamma$  point moved down and became to the CBM, inducing to an indirect-to-direct bandgap transition at a compressive strain of  $\delta = \sim 5\%$  (Figure 2d). Interestingly, this transition is also observed in the 2L  $\alpha$ -NP at ~8% compressive strain (Figure 2e) and in the 3L  $\alpha$ -NP at a compressive strain of  $\sim 12\%$  (Figure 2f). Such controllable direct band gap properties of these  $\alpha$ -NP sheets, easily achieved via strain engineering, significantly increase their potentials for photovoltaics applications. Remarkably, the tunable direct-gap range of our  $\alpha$ -NP sheets covers almost the whole visible-light region when the band gaps are computed within the more accurate HSE functional. In particular, the band-gap for the 3L  $\alpha$ -NP has an ideal value

of 1.34 eV, located almost perfectly within the band gap range (1.2–1.6 eV) that best promotes efficient photoelectric energy conversion. The tunable direct bandgap in the 3L  $\alpha$ -NP suggests its high solar energy conversion efficiency.

The conduction band (CB) and valence band (VB) in the above calculated band structures of 1L, 2L, and 3L  $\alpha$ -NP sheets all are rather dispersive, similar to the situation in BP, which implies their potential high carrier mobilities. Thus, we calculated their carrier mobilities using the deformation potential (DP) theory proposed by Bardeen and Shockley, State of the s which provides information on the carrier transfer capacity in different directions (Figures S9 and S10). Table 1 summarizes the calculated deformation-potential constant  $(E_d^{\alpha})$ , elastic modulus (C2D), effective mass  $(m^*)$ , and carrier mobility  $(\mu)$ . Our calculations indicate that  $\mu$  strongly depends on the layernumber of  $\alpha$ -NP sheets and exhibits anisotropic in the zigzag (x) and armchair (y) directions. In the sheets, the electron mobility in the *x* direction is more than tens of times that along the y direction, and hole's mobility along the y direction is greater than that in the x direction. Among these sheets, the 3L  $\alpha$ -NP possesses the highest  $\mu$  compared to its 1L and 2L counterparts, which is ascribed to its smaller  $m^*$  and higher  $C^{2D}$ . The carrier mobilities of 3L  $\alpha$ -NP are as high as  $\mu_x = 1.1$ imes 10<sup>4</sup> cm<sup>2</sup> V<sup>-1</sup> s<sup>-1</sup> for electrons along the x direction and  $\mu_y$  =  $4.2 \times 10^4$  cm<sup>2</sup> V<sup>-1</sup> s<sup>-1</sup> for holes along the y direction, which are of the same order of magnitude as the mobilities in BP ( $\sim 10^4$ cm<sup>2</sup> V<sup>-1</sup> s<sup>-1</sup>).<sup>55</sup> However, in stark contrast to BP, whose carrier mobility reduces sharply from its monolayer to its few-layer counterpart, the  $\alpha$ -NP multilayer has enhanced hole mobility along the y direction, suggesting that ascendant high mobility can be obtained in a thicker  $\alpha$ -NP multilayer. Among the BP derivatives, such as hittorfene,<sup>56</sup> 2D InP<sub>3</sub>,<sup>57</sup> and 2D CaP<sub>3</sub>,<sup>58</sup> our 3L  $\alpha$ -NP possesses a comparable high hole mobility; thus, it is also expected to be an excellent acceptor material for optoelectronic applications.

Good optical absorption is also essential for photovoltaic applications. Thus, we calculated the absorption coefficients for these 1L, 2L, and 3L  $\alpha$ -NP sheets. As shown in Figure 3a, the absorption coefficients of  $\alpha$ -NP sheets can reach the order of ×10<sup>5</sup> cm<sup>-1</sup>, covering a wide wavelength range in the visible light region. Note that the excitonic effects due to the electron-hole interactions, which are not included in our calculations, may influence the absorption spectra of the  $\alpha$ -NP sheets. Previous studies showed that when electron-hole interactions are considered, the absorption spectra of 2D structures, such as graphene, 59 MoS<sub>2</sub>, and BP, 51 usually have a large exciton binding energy (e.g., 0.96 eV for graphene, 1.1 eV for MoS<sub>2</sub>) with a redshift (Figure S11). Thus, we expect that, by the electron-hole interactions, the absorption spectra of the  $\alpha$ -NP sheets may have a similar redshift and broaden its absorption in the visible light region. Remarkably, the optical absorption coefficients along the in- and out-of-plane directions increase with the number of layers, and the 3L  $\alpha$ -NP shows excellent absorption, reaching a maximum value along the in-plane direction, which is of the same order of magnitude as that of BP and comparable to that of BP's derivative (e.g., 2D GeP<sub>3</sub><sup>18</sup>). In addition, because of the larger cross-section, the in-plane absorptions of these  $\alpha$ -NP sheets are bigger than the corresponding out-of-plane absorptions in the energy region. Such outstanding optical performance for these  $\alpha$ -NP sheets further indicates their promise as efficient photovoltaic solar cell materials.

For a practical solar cell, the photovoltaic efficiency also depends on the thickness of the absorber layer. Here, adopting a Shockley-Queisser model, 62 we calculated the spectroscopic limited maximum efficiency (SLME) of the  $\alpha$ -NP sheets for a standard AM1.5 G solar spectrum at room temperature to evaluated its photovoltaic efficiencies. The same computations were performed for BP and bulk silicon (c-Si) for comparison. As seeing in Figure 3b, as the thickness of these sheets in the  $0-3.0 \mu m$  range, their photovoltaic efficiencies all gradually increases. The SLME of  $\alpha$ -NP sheets is much higher than that of the commercially used c-Si for any given thickness. For example, the  $\alpha$ -NP can achieve a high photovoltaic efficiency of  $\sim 14$  % at a film thickness of  $\sim 1$   $\mu$ m. Notably, the photovoltaic efficiency of  $\alpha$ -NP absorbers is dependent on their thickness. Thus, a high photovoltaic efficiency close to that of BP can be expected as the  $\alpha$ -NP multilayer gets thicker.

In a photovoltaic device design, such as heterostructure solar cell, band offsets across different 2D semiconductors is important and necessary parameter. Accordingly, we investigated the band offsets of 3L  $\alpha$ -NP and 2D transition-metal dichalcogenides (TMDS). Encouragingly, the band alignment between 3L  $\alpha$ -NP and selected TMDS monolayers (Figure 3c) are suitable for potential applications in optoelectronics and solar cells, in which electron-hole pair could be intensively separated. Taking  $WTe_2$ -Mo $Te_2$ -3L  $\alpha$ -NP heterostructure (Figure 3d) as an example, we expect that this heterostructure favors charge carrier separation upon irradiation, where the photoinduced electron is injected from the CB of WTe<sub>2</sub> into the CB of MoTe<sub>2</sub>, and into the CB of 3L  $\alpha$ -NP, while the redundant holes of the 3L  $\alpha$ -NP should be transferred to the VB of WTe<sub>2</sub> and MoTe<sub>2</sub>. Note that this high probability of electron-hole separation could further enhance the high photovoltaic efficiency, which provides a possible way of designing photovoltaic cell with the band alignments engineer-

To confirm our above expectation, we constructed and theoretically examined the fixed type-II heterostructures of MoTe<sub>2</sub>/3L  $\alpha$ -NP as shown in Figure 4a–4c. The important parameter PCE, the fraction of incident solar energy which is converted to electricity in a solar cell device, was estimated according to the model proposed by Bernardi and Scharber. Remarkably, the PCE of MoTe<sub>2</sub>/3L  $\alpha$ -NP has a maximum value of ~16% (Figure 4d), which is much higher than that of marketing solar cells (~9%), <sup>64</sup> and competitive with the values of recently reported MoS<sub>2</sub>/bilayer BP heterostructure (18%), <sup>49</sup> the g-SiC<sub>2</sub> systems (12–20%), <sup>65</sup> C-based photovoltaics (9–13%), <sup>66</sup> and the  $\alpha$ -AsP/GaN bilayer heterojunctions (~22%). This simulation confirms that the  $\alpha$ -AsP sheets-based heterojunctions have a high photovoltaic efficiency in the solar cell applications.

Mechanical cleavage from bulk material is a common method for the preparation of 2D materials. To assess the feasibility of this approach for the 2D  $\alpha$ -NP sheets, we firstly explored the bulk structure of an appropriate (N: P = 1:1) NP compound using extensive PSO structure searches at normal temperature and pressure (Figure 5a) and found that the lower energies crystalline phases (Table S1) are favored to possess layered character, and each layer perfectly comprises our predicted  $\alpha$ -NP configuration (Figure S9). Among them, the  $Cmc2_1$  phase is energetically most favorable (Figure S10) and corresponds to a bulk structure with stacked 2D  $\alpha$ -NP sheets.

We then evaluated the feasibility to prepare the  $Cmc2_1$  phase of NP compound. To our best knowledge, the  $P_3N_5$  compound

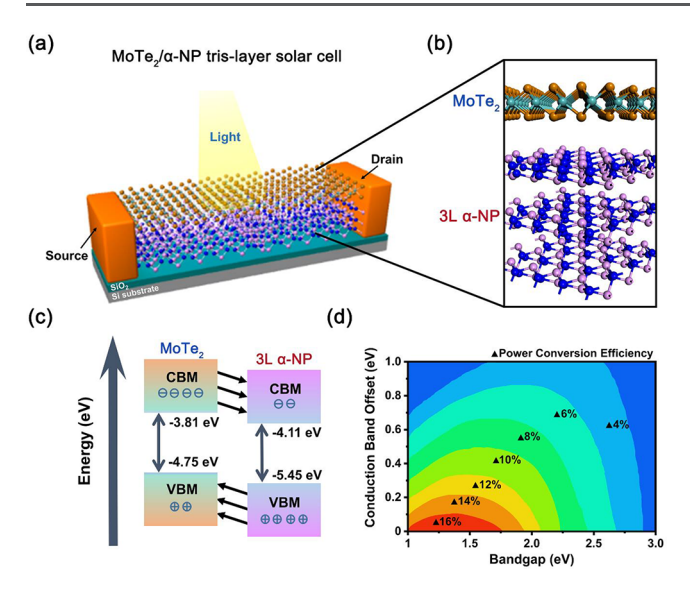


Figure 4. (a) Schematic of the MoTe<sub>2</sub>/3L  $\alpha$ -NP heterostructure solar cell. (b) The heterostructure of the MoTe<sub>2</sub>/3L  $\alpha$ -NP. (c) Schematic drawing CBM and VMB of MoTe<sub>2</sub>/3L  $\alpha$ -NP heterostructure, where the 3L  $\alpha$ -NP sheets is assumed to an ideal direct-bandgap case and the MoTe<sub>2</sub> monolayer meets the requirement for type-II heterostructure with the 3L  $\alpha$ -NP. (d) The calculated PCE of MoTe<sub>2</sub>/3L  $\alpha$ -NP heterostructure.

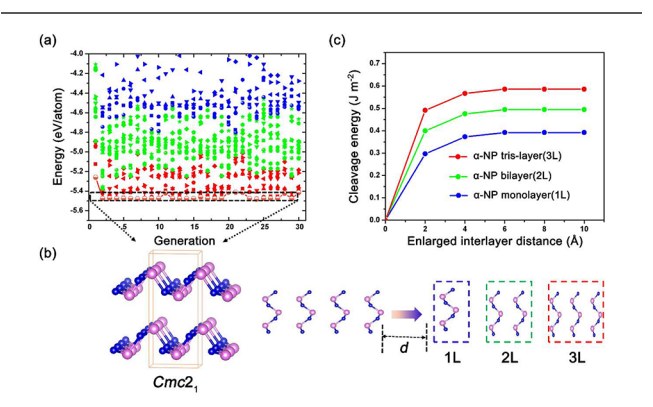


Figure 5. (a) Total energies for predicted 3D NP structures as the function of generations. The RGB color coding represents the different energy orders. (b) The bulk crystal structure of  $Cmc2_1$  phase and schematic showing mechanical cleavage of the bulk. (c) The calculated cleavage energy of 1L, 2L, and 3L  $\alpha$ -NP sheets as the function of the interlayer distance d.

is only synthesized N-P crystal at normal condition.<sup>67</sup> Thus, we evaluated the stability of the Cmc2<sub>1</sub> phase relative to black P, P<sub>3</sub>N<sub>5</sub>, and molecular N<sub>2</sub> compositions. At normal conditions, it found that the reaction route P + 1/2  $N_2 \rightarrow$ NP with a positive Gibbs free energy values indicate that it is unlikely to synthesize NP using molecular N2 as a precursor under normal conditions, mostly because of the strong binding energy in the N<sub>2</sub> triple bond. Nevertheless, the N<sub>2</sub> triple bond can be easily broken under high pressure. For example, solid He and molecular N<sub>2</sub> are predicted to form an energeticallystable compound with stoichiometry HeN<sub>4</sub>, and no N triple bonds are available at pressures above 8.5 GPa.<sup>68</sup> This highpressure technology may help synthesize this NP compound. To check this route, we further calculated the formation enthalpy  $(\Delta H)$  of our NP structure with respect to  $N_2 + P$  and 2P + P<sub>3</sub>N<sub>5</sub> at an elevated pressure range of 0–20 GPa (Figure

S11) and found that the NP compound could be synthesized at above  $\sim$ 10 GPa.

Subsequently, to explore the feasibility of exfoliating the  $\alpha$ -NP sheets from the bulk layered Cmc21 structure, using a sixlayer slab model, we calculated the cleavage energies of 1L, 2L, and 3L  $\alpha$ -NP sheets. The variation in total energy as a function of the separation distance, d, between the fixed layers and the flexible layers was calculated to simulate the exfoliation process (Figure 5b). Increasing the distance between the exfoliated 1L, 2L, or 3L and the bulk increases the energy, which convergences at a distance of ~6 Å (Figure 5c). The cleavage energies for 1L, 2L, and 3L  $\alpha$ -NP sheets are  $\sim$ 0.39, 0.47, and 0.58 J m<sup>-2</sup>, respectively, which are in the same range of the experimentally estimated exfoliation energy of BP (0.37 J m<sup>-2</sup>).<sup>69</sup> These data suggest that the  $\alpha$ -NP sheets can also be easily produced from its bulk phase by exfoliation. Within the present ab initio framework, we anticipate that the  $\alpha$ -NP sheets can be exfoliated from the bulk NP compound that may be synthesizable at high pressure.

In conclusion, we have identified the most stable  $N_x P_{1-x}$ monolayer compound that exists in the N-P binary system, using the PSO algorithm combined with DFT calculations. The N: P = 1:1 composition with a BP-like  $\alpha$ -NP structure is thermodynamically favorable. Phonon calculations and AIMD simulations confirmed that the  $\alpha$ -NP sheet is dynamically, thermally, and chemically stable. Interestingly, the few-layer  $\alpha$ -NP sheets are semiconducting with a highly tunable direct band gap under the compressive strain and possess very high electron mobility and absorption coefficient depending on the number of layers. In particular, the carrier mobilities of the 3L  $\alpha$ -NP can be as high as 1.1  $\times$  10<sup>4</sup> cm<sup>2</sup> V<sup>-1</sup> s<sup>-1</sup> for electrons along the x direction and  $4.2 \times 10^4$  cm<sup>2</sup> V<sup>-1</sup> s<sup>-1</sup> for holes along the y direction, with excellent absorption coefficients of  $\sim 10^{\circ}$ cm<sup>-1</sup>. These properties suggest these  $\alpha$ -NP sheets may be very promising materials for high-efficiency solar cells, as demonstrate by the estimated photovoltaic efficiency of ~14 % at a film thickness of 1  $\mu$ m. Meanwhile, an ideal type-II heterostructure made of MoTe<sub>2</sub> and 3L  $\alpha$ -NP is revealed to reach a conversion efficiency up to ~16%. Our work also indicate that it is highly feasible to prepare the  $\alpha$ -NP sheets by mechanical cleavage from its bulk NP compound. Once synthesized, the  $\alpha$ -NP sheets may give a new platform for BPlike material and superior photovoltaic applications.

# ASSOCIATED CONTENT

# Supporting Information

The Supporting Information is available free of charge on the ACS Publications website at DOI: 10.1021/acsmaterial-slett.9b00220.

Details of structure prediction, the calculated methods of carrier mobility, absorption coefficients, and power conversion efficient, phonon spectra, AIMD simulations, ELF, and DOS of  $\alpha$ -NP monolayer, structural parameters and relative stability for bulk  $Cmc2_1$ -NP structure, band structure and band gap by strain of  $\alpha$ -NP monolayer, and details for the calculations of the carrier mobilities for the 1L, 2L, and 3L  $\alpha$ -NP sheets according to the DP theory (PDF)

## AUTHOR INFORMATION

# **Corresponding Authors**

\*E-mail: cyz@calypso.org.cn or cyz@swjtu.edu.cn.

\*E-mail: xf232@cam.ac.uk.

\*E-mail: zhongfangchen@gmail.com.

#### ORCID ®

Yuanzheng Chen: 0000-0001-5467-536X

Bai Sun: 0000-0002-5840-509X

Simon A. T. Redfern: 0000-0001-9513-0147 Zhongfang Chen: 0000-0002-1445-9184

# **Author Contributions**

Y.C., Z.L., and B.S. contributed equally.

### Notes

The authors declare no competing financial interest.

# ACKNOWLEDGMENTS

We acknowledge the support of the National Natural Science Foundation of China (11604270, 11704050), the Fundamental Research Funds for the Central Universities in China (2682017CX052 and 2018GF08), the USA NSF-CREST Center for Innovation, Research and Education in Environmental Nanotechnology (CIRE2N) (Grant Number HRD-1736093), and the UK Natural Environment Research Council under grant NE/P012167/1.

## REFERENCES

- (1) Petter Jelle, B.; Breivik, C.; Drolsum Røkenes, H. Building integrated photovoltaic products: A state-of-the-art review and future research opportunities. Sol. Energy Mater. Sol. Cells 2012, 100, 69–96.
- (2) Green, M. A. Crystalline and thin-film silicon solar cells, state of the art and future potential. *Sol. Energy* **2003**, *74*, 181–192.
- (3) Ginley, D.; Green, M. A.; Collins, R. Solar energy conversion toward 1 terawatt. MRS Bull. 2008, 33, 355–364.
- (4) Hao, L.; Liu, Y.; Gao, W.; Han, Z.; Xue, Q.; Zeng, H.; Wu, Z.; Zhu, J.; Zhang, W. Electrical and photovoltaic characteristics of MoS<sub>2</sub>/Si pn junctions. *J. Appl. Phys.* **2015**, *117*, 114502.
- (5) Nagamatsu, K. A.; Avasthi, S.; Jhaveri, J.; Sturm, J. C. A 12% efficient silicon/PEDOT, PSS heterojunction solar cell fabricated at< 100 C. *IEEE J. Photovolt.* **2014**, *4*, 260–264.
- (6) Kim, D. Y.; Santbergen, R.; Tan, H.; van Swaaij, R. A. C. M. M.; Smets, A. H. M.; Isabella, O.; Zeman, M. Quadruple-junction thin-film silicon-based solar cells with high open-circuit voltage. *Appl. Phys. Lett.* **2014**, *105*, 063902.
- (7) Zhan, X.; Tan, Z.; Domercq, B.; An, Z.; Zhang, X.; Barlow, S.; Li, Y.; Zhu, D.; Kippelen, B.; Marder, S. R. A high-mobility electron-transport polymer with broad absorption and its use in field-effect transistors and all-polymer solar cells. *J. Am. Chem. Soc.* **2007**, *129*, 7246–7247.
- (8) Zhou, E.; Cong, J.; Wei, Q.; Tajima, K.; Yang, C.; Hashimoto, K. All-polymer solar cells from perylene diimide based copolymers: material design and phase separation control. *Angew. Chem., Int. Ed.* **2011**, *50*, 2799–2803.
- (9) Facchetti, A. Polymer donor-polymer acceptor (all-polymer) solar cells. *Mater. Today* **2013**, *16*, 123–132.
- (10) Linghu, J.; Yang, T.; Luo, Y. Z.; Yang, M.; Zhou, J.; Shen, L.; Feng, Y. P. High-Throughput Computational Screening of Vertical 2D van der Waals Heterostructures for High-efficiency Excitonic Solar Cells. ACS Appl. Mater. Interfaces 2018, 10, 32142–32150.
- (11) Geim, A. K.; Novoselov, K. S. Detection of individual gas molecules adsorbed on graphene. *Nat. Mater.* **2007**, *6*, 183–191.
- (12) Bernardi, M.; Palummo, M.; Grossman, J. C. Semiconducting monolayer materials as a tunable platform for excitonic solar cells. *ACS Nano* **2012**, *6*, 10082–10089.
- (13) Li, L.; Yu, Y.; Ye, G. J.; Ge, Q.; Ou, X.; Wu, H.; Feng, D.; Chen, X. H.; Zhang, Y. Black phosphorus field-effect transistors. *Nat. Nanotechnol.* **2014**, *9*, 372–377.

- (14) Liu, H.; Neal, A. T.; Zhu, Z.; Luo, Z.; Xu, X.; Tomanek, D.; Ye, P. D. Phosphorene: an unexplored 2D semiconductor with a high hole mobility. *ACS Nano* **2014**, *8*, 4033–4041.
- (15) Das, S.; Zhang, W.; Demarteau, M.; Hoffmann, A.; Dubey, M.; Roelofs, A. Tunable transport gap in phosphorene. *Nano Lett.* **2014**, *14*, *5733*–*5739*.
- (16) Zhou, Q.; Chen, Q.; Tong, Y.; Wang, J. Light-induced ambient degradation of few-layer black phosphorus: mechanism and protection. *Angew. Chem., Int. Ed.* **2016**, *55*, 11437.
- (17) Xie, M.; Zhang, S.; Cai, B.; Huang, Y.; Zou, Y.; Guo, B.; Zeng, H.; et al. A promising two-dimensional solar cell donor: Black arsenic–phosphorus monolayer with 1.54 eV direct bandgap and mobility exceeding 14 000 cm<sup>2</sup> V<sup>-1</sup> s<sup>-1</sup>. *Nano Energy* **2016**, *28*, 433–439
- (18) Jing, Y.; Ma, Y.; Li, Y.; Heine, T. GeP<sub>3</sub>: A Small Indirect Band Gap 2D Crystal with High Carrier Mobility and Strong Interlayer Quantum Confinement. *Nano Lett.* **2017**, *17*, 1833–1838.
- (19) Sun, S.; Meng, F.; Wang, H.; Wang, H.; Ni, Y. Novel two-dimensional semiconductor SnP<sub>3</sub>: high stability, tunable bandgaps and high carrier mobility explored using first-principles calculations. *J. Mater. Chem. A* **2018**, *6*, 11890–11897.
- (20) Li, L.; Wang, W.; Gong, P.; Zhu, X.; Deng, B.; Shi, X.; Gao, Y.; Li, Q.; Zhai, T. 2D GeP: An Unexploited Low-Symmetry Semiconductor with Strong In-Plane Anisotropy. *Adv. Mater.* **2018**, *30*, 1706771.
- (21) Batmunkh, M.; Bat-Erdene, M.; Shapter, J. G. Phosphorene and Phosphorene-Based Materials-Prospects for Future Applications. *Adv. Mater.* **2016**, 28, 8586.
- (22) Cai, X.; Chen, Y.; Sun, B.; Chen, J.; Wang, H.; et al. Two-dimensional Blue-AsP monolayers with tunable direct band gap and ultrahigh carrier mobility show promising high-performance photovoltaic properties. *Nanoscale* **2019**, *11*, 8260–8269.
- (23) Liu, B.; Köpf, M.; Abbas, A. N.; Wang, X.; Guo, Q.; Jia, Y.; et al. Black arsenic—phosphorus: layered anisotropic infrared semiconductors with highly tunable compositions and properties. *Adv. Mater.* **2015**, 27, 4423.
- (24) Shojaei, F.; Kang, H. S. Partially planar BP<sub>3</sub> with high electron mobility as a phosphorene analog. *J. Mater. Chem. C* **2017**, *5*, 11267–11274.
- (25) Wang, G.; Pandey, R.; Karna, S. P. Carbon phosphide monolayers with superior carrier mobility. *Nanoscale* **2016**, *8*, 8819.
- (26) Boukhvalov, D. W. The atomic and electronic structure of nitrogen-and boron-doped phosphorene. *Phys. Chem. Chem. Phys.* **2015**, *17*, 27210–27216.
- (27) Zhang, X.; Chen, A.; Zhou, Z. High-throughput computational screening of layered and two-dimensional materials. *WIREs Comput. Mol. Sci.* **2019**, *9*, No. e1385.
- (28) Zhang, X.; Zhang, Z.; Wu, D.; Zhang, X.; Zhao, X.; Zhou, Z. Computational screening of 2D materials and rational design of heterojunctions for water splitting photocatalysts. *Small Methods* **2018**, *2*, 1700359.
- (29) Mounet, N.; Gibertini, M.; Schwaller, P.; et al. Two-dimensional materials from high-throughput computational exfoliation of experimentally known compounds. *Nat. Nanotechnol.* **2018**, 13, 246–252.
- (30) Ma, S.; He, C.; Sun, L. Z.; Lin, H.; Li, Y.; Zhang, K. W. Stability of two-dimensional PN monolayer sheets and their electronic properties. *Phys. Chem. Chem. Phys.* **2015**, *17*, 32009–32015.
- (31) Zhao, L.; Yi, W.; Botana, J.; Gu, F.; Miao, M. Nitrophosphorene: A 2D semiconductor with both large direct gap and superior mobility. *J. Phys. Chem. C* **2017**, *121*, 28520–28526.
- (32) Yu, W.; Niu, C.; Zhu, Z.; Wang, X.; Zhang, W. B. Atomically thin binary V–V compound semiconductor: a first-principles study. *J. Mater. Chem. C* **2016**, *4*, 6581.
- (33) Wang, Y.; Lv, J.; Zhu, L.; Ma, Y. Crystal structure prediction via particle-swarm optimization. *Phys. Rev. B: Condens. Matter Mater. Phys.* **2010**, 82, 094116.
- (34) Xu, M.; Shao, S.; Gao, B.; Lv, J.; Li, Q.; Wang, Y.; Wang, H.; Zhang, L.; Ma, Y. Anatase (101)-like Structural Model Revealed for

Metastable Rutile TiO<sub>2</sub>(011) Surface. ACS Appl. Mater. Interfaces 2017, 9, 7891–7896.

- (35) Lv, J.; Wang, Y.; Zhu, L.; Ma, Y. Predicted novel high-pressure phases of lithium. *Phys. Rev. Lett.* **2011**, *106*, 015503.
- (36) Harran, I.; Chen, Y.; Wang, H.; Ni, Y. Pressure induced evolution of structures and properties of iron tetraboride. *CrystEngComm* **2018**, *20*, 3928–3935.
- (37) Wang, H.; Tse, J. S.; Tanaka, K.; Iitaka, T.; Ma, Y. Superconductive sodalite-like clathrate calcium hydride at high pressures. *Proc. Natl. Acad. Sci. U. S. A.* **2012**, *109*, 6463–6466.
- (38) Chen, Y.; Cai, X.; Wang, H.; Wang, H.; Wang, H. Novel triadius-like N<sub>4</sub> specie of iron nitride compounds under high pressure. *Sci. Rep.* **2018**, *8*, 10670.
- (39) Zhu, L.; Liu, H.; Pickard, C. J.; Zou, G.; Ma, Y. Reactions of xenon with iron and nickel are predicted in the Earth's inner core. *Nat. Chem.* **2014**, *6*, 644–648.
- (40) Harran, I.; Chen, Y.; Wang, H.; Li, H.; Li, Y.; Tao, L. High-pressure induced phase transition of FeS<sub>2</sub>: Electronic, mechanical and thermoelectric properties. *J. Alloys Compd.* **2017**, *710*, 267–273.
- (41) Chen, Y.; Feng, X.; Chen, J.; Cai, X.; Sun, B.; Wang, H.; Du, H.; Redfern, S. A. T.; Xie, Y.; Liu, H. Ultrahigh-pressure induced decomposition of silicon disulfide into silicon-sulfur compounds with high coordination numbers. *Phys. Rev. B* **2019**, *99*, 184106.
- (42) Kresse, G.; Furthmüller, J. Efficient iterative schemes for ab initio total-energy calculations using a plane-wave basis set. *Phys. Rev. B: Condens. Matter Mater. Phys.* **1996**, *54*, 11169.
- (43) Dion, M.; Rydberg, H.; Schröder, E.; Langreth, D. C.; Lundqvist, B. I. Van der Waals density functional for general geometries. *Phys. Rev. Lett.* **2004**, *92*, 246401.
- (44) Heyd, J.; Scuseria, G. E.; Ernzerhof, M. Hybrid functionals based on a screened Coulomb potential. *J. Chem. Phys.* **2003**, *118*, 8207–8215.
- (45) Togo, A.; Oba, F.; Tanaka, I. First-principles calculations of the ferroelastic transition between rutile-type and CaCl<sub>2</sub>-type SiO<sub>2</sub> at high pressures. *Phys. Rev. B: Condens. Matter Mater. Phys.* **2008**, *78*, 134106.
- (46) Özcelik, V. O.; Aktürk, O. Ü.; Durgun, E.; Ciraci, S. Single-layer crystalline phases of antimony: Antimonenes. *Phys. Rev. B: Condens. Matter Mater. Phys.* **2015**, 92, 125420.
- (47) Born, M.; Kun, H. Dynamical Theory of Crystal Lattices; Clarendon Press, 1954.
- (48) Lui, C. H.; Li, Z.; Mak, K. F.; Cappelluti, E.; Heinz, T. F. Observation of an electrically tunable band gap in trilayer graphene. *Nat. Phys.* **2011**, *7*, 944–947.
- (49) Dai, J.; Zeng, X. C. Bilayer phosphorene: effect of stacking order on bandgap and its potential applications in thin-film solar cells. *J. Phys. Chem. Lett.* **2014**, *5*, 1289–1293.
- (50) Xie, M.; Zhang, S.; Cai, B.; Gu, Y.; Liu, X.; Kan, E.; Zeng, H. Van der Waals bilayer antimonene: a promising thermophotovoltaic cell material with 31% energy conversion efficiency. *Nano Energy* **2017**, *38*, 561–568.
- (51) Susner, M. A.; Chyasnavichyus, M.; McGuire, M. A.; Ganesh, P.; Maksymovych, P. Metal Thio-and Selenophosphates as Multifunctional van der Waals Layered Materials. *Adv. Mater.* **2017**, 29, 1602852.
- (52) Kamal, C.; Ezawa, M. Two-dimensional buckled and puckered honeycomb arsenic systems. *Phys. Rev. B: Condens. Matter Mater. Phys.* **2015**, *91*, 085423.
- (53) Shockley, W.; Queisser, H. J. Detailed Balance Limit of Efficiency of p-n Junction Solar Cells. *J. Appl. Phys.* **1961**, 32, 510–519.
- (54) Bardeen, J.; Shockley, W. Deformation potentials and mobilities in non-polar crystals Deformation potentials and mobilities in non-polar crystals. *Phys. Rev.* **1950**, *80*, 72–80.
- (55) Qiao, J.; Kong, X.; Hu, Z. X.; Yang, F.; Ji, W. High-mobility transport anisotropy and linear dichroism in few-layer black phosphorus. *Nat. Commun.* **2014**, *5*, 4475.

(56) Schusteritsch, G.; Uhrin, M.; Pickard, C. J. Single-Layered Hittorf's Phosphorus: A Wide-Bandgap High Mobility 2D Material. *Nano Lett.* **2016**, *16*, 2975–2980.

- (57) Miao, N.; Xu, B.; Bristowe, N. C.; Zhou, J.; Sun, Z. Tunable magnetism and extraordinary sunlight absorbance in indium triphosphide monolayer. *J. Am. Chem. Soc.* **2017**, *139*, 11125–11131.
- (58) Lu, N.; Zhuo, Z.; Guo, H.; Wu, P.; Fa, W.; Wu, X.; Zeng, X. C. CaP<sub>3</sub>: A New Two-Dimensional Functional Material with Desirable Band Gap and Ultrahigh Carrier Mobility. *J. Phys. Chem. Lett.* **2018**, *9*, 1728–1733.
- (59) Qiu, D. Y.; da Jornada, F. H.; Louie, S. G. Optical spectrum of MoS<sub>2</sub>: many-body effects and diversity of exciton states. *Phys. Rev. Lett.* **2013**, *111*, 216805.
- (60) Yang, L.; Deslippe, J.; Park, C. H.; Cohen, M. L.; Louie, S. G. Excitonic effects on the optical response of graphene and bilayer graphene. *Phys. Rev. Lett.* **2009**, *103*, 186802.
- (61) Villegas, C. E.; Rodin, A. S.; Carvalho, A.; Rocha, A. R. Twodimensional exciton properties in monolayer semiconducting phosphorus allotropes. *Phys. Chem. Chem. Phys.* **2016**, *18*, 27829.
- (62) Yu, L.; Zunger, A. Identification of potential photovoltaic absorbers based on first-principles spectroscopic screening of materials. *Phys. Rev. Lett.* **2012**, *108*, 68701.
- (63) Scharber, M. C.; Mühlbacher, D.; Koppe, M.; Denk, P.; Waldauf, C.; Heeger, A. J.; Brabec, C. J. Design rules for donors in bulk-heterojunction solar cells—Towards 10% energy-conversion efficiency. *Adv. Mater.* **2006**, *18*, 789–794.
- (64) Green, M. A.; Emery, K.; Hishikawa, Y.; Warta, W.; Dunlop, E. D.; Levi, D. H.; Ho-Baillie, A. W. Y. Solar cell efficiency tables (Version 45). *Prog. Photovoltaics* **2017**, *25*, 3–13.
- (65) Zhou, L. J.; Zhang, Y. F.; Wu, L. M. SiC<sub>2</sub> Siligraphene and Nanotubes: Novel Donor Materials in Excitonic Solar Cells. *Nano Lett.* **2013**, *13*, 5431–5436.
- (66) Bernardi, M.; Lohrman, J.; Kumar, P. V.; Kirkeminde, A.; Ferralis, N.; Grossman, J. C.; Ren, S. Nanocarbon-based photovoltaics. *ACS Nano* **2012**, *6*, 8896–8903.
- (67) Kroll, P.; Schnick, W. Density Functional Study of Phosphorus Nitride  $P_3N_5$ : Refined Geometries, Properties, and Relative Stability of  $\alpha$ - $P_3N_5$  and  $\gamma$ - $P_3N_5$  and a Further Possible High-Pressure Phase - $P_3N_5$  with Kyanite-Type Structure. *Chem. Eur. J.* **2002**, *8*, 3530–3537
- (68) Li, Y.; Feng, X.; Liu, H.; Hao, J.; Redfern, S. A. T.; Lei, W.; Liu, D.; Ma, Y. Route to high-energy density polymeric nitrogen tN via He— N compounds. *Nat. Commun.* **2018**, *9*, 722.
- (69) Zacharia, R.; Ulbricht, H.; Hertel, T. Interlayer cohesive energy of graphite from thermal desorption of polyaromatic hydrocarbons. *Phys. Rev. B: Condens. Matter Mater. Phys.* **2004**, *69*, 155406.